Journal of Materials Chemistry C

PAPER

View Article Online
View Journal | View Issue

Cite this: J. Mater. Chem. C, 2014, 2, 5660

Ultrafast chemical dynamic behavior in highly epitaxial $LaBaCo_2O_{5+\delta}$ thin films

H. B. Wang,†[ab] S. Y. Bao,†[a] J. Liu,[a] G. Collins,[a] C. R. Ma,[a] M. Liu,[ac] C. L. Chen,*[ad] C. Dong,[b] M.-H. Whangbo,[e] H. M. Guo[f] and H. J. Gao[f]

Received 12th March 2014
Accepted 24th April 2014

DOI: 10.1039/c4tc00492b

www.rsc.org/MaterialsC

The redox reactions of highly epitaxial $LaBaCo_2O_{5+\delta}$ (LBCO) thin films exposed to the switching flow of reducing (H_2) and oxidizing (O_2) gases were examined at various temperatures between 260 and 700 °C. Their electrical resistance was measured using a precise ac bridge measurement system. The as-grown LBCO films have very good electrical conductivity at low and medium temperatures between 400 and 700 °C, and are extremely sensitive to reducing and oxidizing environments with superfast redox dynamics. The LBCO thin films show more complex redox reactions at low temperatures (300–350 °C), suggesting the occurrence of conducting-to-insulating-to-conducting transitions during the redox reactions. In particular, the insulating-to-conducting transition under an oxidation process is superfast, with the largest resistance change of up to $3 \times 10^7\ \Omega\ s^{-1}$, occurring even at a low temperature of 300 °C. The extremely short response time, the giant resistance change, and the excellent chemical stability in a broad temperature range from 260 to 700 °C suggests that the highly epitaxial LBCO thin-films can be excellent candidates for low-temperature solid oxide fuel cells, chemical sensors, and catalyst applications.

1. Introduction

Recently 112-type cobalt oxides, $LnBaCo_2O_{5.5}$ (LnBCO) (Ln = rare earth), with perovskite structures have become a subject of intense studies, both theoretically and experimentally, due to their unusual magnetic and electrical transport properties.[1–4] The structure of the double-perovskite $LnBaCo_2O_{5+\delta}$ has a layer sequence of $[LnO_\delta][CoO_2][BaO]\ [CoO_2]$ along the c axis. With an ideal oxygen stoichiometry of 5.5 per formula unit (*i.e.*, $\delta = 0.5$), the average oxidation state of Co is +3. $LnBaCo_2O_{5+\delta}$ with different extents of oxygen deficiency gives rise to ordered, nano-ordered, and disordered phases. The ionic and electronic conductivities of $LnBaCo_2O_{5+\delta}$ depend on the extent of oxygen deficiency, thereby leading to a family of mixed ionic and electronic conducting materials with different physical and chemical properties.[5–10] Taskin *et al.* observed that the A-site ordered $GdBaCo_2O_{5.5+\delta}$ significantly enhances oxygen diffusivity.[11] Previous studies have found that the A-site ordered $PrBaCo_2O_{5.5+\delta}$ exhibits ultrafast oxygen transport kinetics at low temperatures ranging from 300 to 500 °C.[12–14] The size difference between La^{3+} and Ba^{2+} ions is small, which makes ordering of these ions difficult, however, ordered 112-type $LaBaCo_2O_{5+\delta}$ (LBCO) can be prepared under specific synthesis conditions. Rautama *et al.* successfully fabricated and characterized the nanoscale-ordered and disordered forms of fully oxidized $LaBaCo_2O_6$ as well as the ordered form of the oxygen-deficient $LaBaCo_2O_{5.5}$.[15,16] With different synthesis methods, many studies have found that the oxygen content in the Ln/Ba ordered perovskite $LnBaCo_2O_x$ can be varied from $x = 6$ to $x = 4.5$, which leads to a change in the average cobalt oxidation state from +3.5 to +2.[17,18] In addition, Seddon *et al.* found that the ground samples of $YBaCo_2O_5$ and $LaBaCo_2O_5$ are reduced by strongly reducing NaH to form $YBaCo_2O_{4.5}$ and $LaBaCo_2O_{4.25}$, respectively.[19] Recently, we have successfully obtained the highly epitaxial LnBCO thin films and systematically studied the epitaxial nature and their electrical transport, magnetic and chemical properties.[20–28] When these films are exposed to the switching flow of reducing (4% H_2 + 96% N_2, which will be referred to as H_2 for simplicity) and oxidizing (O_2) gases, their electrical resistance exhibits an ultrafast and dramatic change at a very broad temperature range, varying from 400 to 800 °C, which reflects the change in the oxidation states of the cobalt atoms under the different redox environments.[29] In this paper, we carry out resistance measurements on the highly epitaxial

[a]Department of Physics and Astronomy, University of Texas at San Antonio, TX 78249, USA. E-mail: cl.chen@utsa.edu

[b]School of Materials Science and Engineering, Dalian University of Technology, Dalian 116024, China

[c]Electronic Materials Research Laboratory, Xi'an Jiaotong University, Xi'an 710049, P.R. China

[d]The Texas Canter for Superconductivity, University of Houston, Houston, Texas 77204, USA

[e]Department of Chemistry, North Carolina State University, Raleigh, North Carolina 27695-8204, USA

[f]Institute of Physics, Chinese Academy of Sciences, Beijing 100080, China

† Wang and Bao contributed equally to this work.

LBCO thin films under the switching flow of H_2 and O_2 gases in the temperature range of 260–800 °C, in order to find the occurrence of a conducting-to-insulating transition at medium temperatures (400–700 °C) and a conducting-to-insulating-to-conducting transition at lower temperatures (300 and 350 °C). These observations are expected to be of potential importance when developing up-to-date low temperature SOFC cathodes, chemical sensors and vehicle exhaust catalysts.

2. Experiments

LBCO thin films were epitaxially grown on (001) $LaAlO_3$ (LAO) single crystal ($c_{LAO} = 0.3788$ nm) substrates using a KrF excimer (at a wavelength of 248 nm) pulsed laser deposition (PLD) system. An energy density of 2.0 J cm^{-2} and a laser repetition rate of 5 Hz were adopted during the film deposition. A high density, single phase, stoichiometric $(LaBa)Co_2O_{5+\delta}$ target was purchased from MTI Crystal Inc. Highly epitaxial LBCO thin films were produced under optimized growth conditions at 850 °C and at an oxygen pressure of 250 mTorr. The as-grown films were annealed *in situ* in 200 Torr oxygen for 15 min at 850 °C, and cooled down to room temperature at a rate of 5 °C min^{-1}. The microstructure and crystallinity of the as-grown LBCO films were examined by a routing X-ray diffraction technique and characterized by cross sectional and plan-view transmission electron microscopy, details of which are given in a previous report.[19] The chemical dynamic measurements on the LBCO films were conducted using a Lake Shore 370 AC Precise Resistance Bridge System at temperatures ranging from 260 to 700 °C, under pure oxygen or a mixture of 5% hydrogen and 95% nitrogen (H–N mixture), and at a pressure of 1 atm. The platinum leads were glued on the film surface with high temperature silver paste, air-dried at room temperature and then annealed at 800 °C, before measurements were taken.

3. Results and discussion

3.1. Medium temperature transitions

The ac conductivity measurements indicate that at medium temperatures (400–700 °C), the resistance of the LBCO thin films changes drastically during the redox reactions. Under an oxidizing environment of O_2, the LBCO thin films are good electrical conductors with a resistance R less than 1000 Ω. Liu *et al.* studied the temperature dependence of the electrical resistivity of the LBCO thin films and found a linear relationship between $\ln(\rho/T)$ and $1/T$,[20] which corresponds to the resistivity behavior of small polarons.[30] Thus, the conductivity of the LBCO thin films comes from the coexistence of Co^{3+} and Co^{4+} ions according to the mechanism of small-polaron hopping conduction of most mixed-valence transition metal oxides.[31–33] As the gas flow was switched from O_2 to H_2, the Co^{4+} ions were reduced to Co^{3+} ions. As the reduction of the LBCO thin films proceeds, the amount of Co^{4+} decreases, directly lowering the amount of small-polarons which are carriers, and therefore raising the resistance of the LBCO thin films. Finally, almost all Co^{4+} ions were reduced to Co^{3+} ions making the LBCO thin films insulating with a resistance greater than 10^7 Ω. Note that the resistance does not change any more even if the reduction time is increased at a medium temperature above 400 °C. This is different from the low temperature (260–350 °C) phenomenon (see below). The change in resistance R under the switching flow of the reducing/oxidizing gas at 500 °C is shown in Fig. 1(a), and the associated dR/dt in Fig. 1(b). As the gas flow is switched from H_2 to O_2, the oxidation from Co^{3+} to Co^{4+} occurs, and the resistance decreases ultrafast at a rate much greater than the reduction reaction. This indicates that the reduced LBCO thin films have a large number of oxygen vacancies and that the Co^{3+} ions are extremely sensitive to O_2. Furthermore, at 500 °C, the LBCO thin films show excellent chemical stability with good reproducibility of the conducting-to-insulating transitions.

3.2. Low temperature transitions

While monitoring the resistance change during the redox reactions at low temperatures (260–400 °C), we found that the LBCO thin films go through more complex transitions involving three obvious states with a sudden change in the resistance. Fig. 2 shows the R *vs.* t and dR/dt *vs.* t curves at 350 °C. As shown in Fig. 2(a), there is a peak in the R *vs.* t curve during each reduction cycle under H_2 and during each oxidation cycle under O_2. This phenomenon suggests that each transition, between conducting and insulating states, in the early part of the reduction reaction cycle is followed by a transition between insulating and conducting states. These transitions are also reversible through the redox reactions. Under the repetitive switching of the redox environments, the reduction and

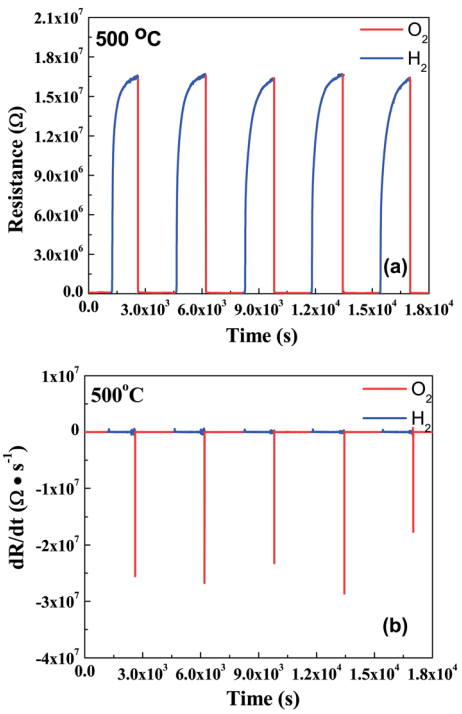

Fig. 1 (a) R *vs.* t and (b) dR/dt *vs.* t curves measured for the LBCO thin films under oxidizing/reducing atmospheres at 500 °C.

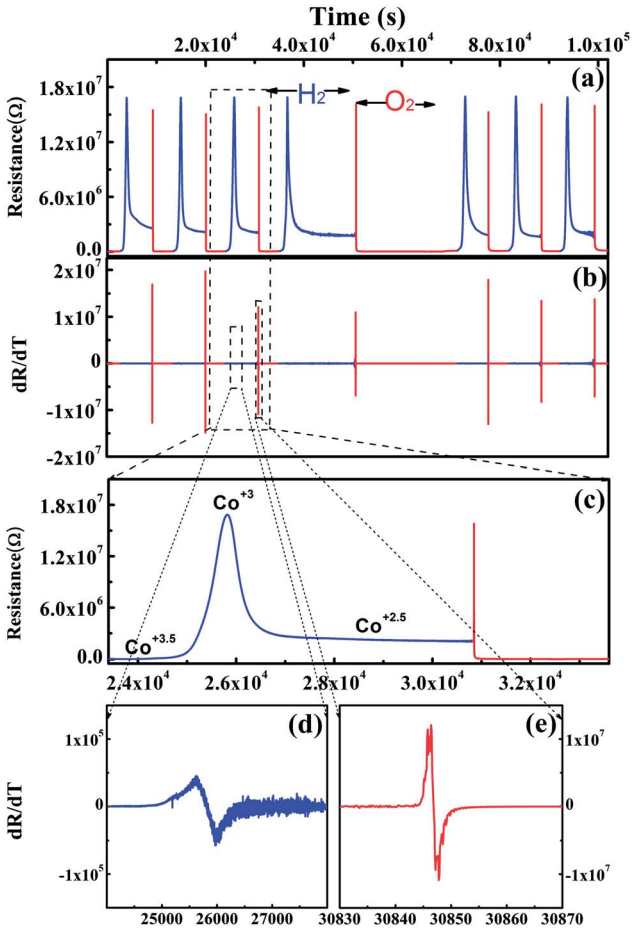

Fig. 2 (a) *R vs. t* and (b) d*R*/d*t vs. t* curves measured for the LBCO thin films under oxidizing/reducing atmospheres measured at 350 °C. (c) A zoomed-in view of the *R vs. t* curve for one oxidation/reduction cycle showing the variation of the Co oxidation state as a function of *t*. The d*R*/d*t vs. t* curves for the (d) reduction and (e) oxidation processes of the reduction/oxidation cycle presented in (c).

oxidation processes of the LBCO films are highly reversible, as can be seen from Fig. 2 for the case of the redox reactions at 350 °C. Fig. 2(b) shows that, as the gas flow is switched from O_2 to H_2, the resistance *R* of LBCO increases to the maximum value and then decreases gradually to the equilibrium value. As the gas flow is switched from H_2 back to O_2, the resistance rapidly reaches its maximum value with a maximum rate of $\sim 10^9\ \Omega\ s^{-1}$ and then quickly decreases to the stable value. These resistance changes are attributed to the average Co oxidation states on the surface of the films. In a pure O_2 environment, LBCO can be fully oxidized to become $ErBaCo_2O_6$ with a Co average oxidation state of +3.5. As the gas flow changes from O_2 to H_2, LBCO is reduced to $LaBaCo_2O_5(OH)$ and then $LaBaCo_2O_{5.5}$ (by losing oxygen in terms of H_2O) with an average Co oxidation state of +3, which explains the sharp increase in the resistance. A further reduction under H_2 changes LBCO to $LaBaCo_2O_{4.5}(OH)$ and then $LaBaCo_2O_5$, with an average Co oxidation state of +2.5, which explains the sharp decrease in the resistance.

Fig. 3(a) and (b) show the detailed *R vs. t* measurements for the reduction and oxidation cycles at various temperatures, which indicate that at a given temperature the resistance change of the LBCO films under oxidation is much faster than that under reduction. When the gas flow is switched from H_2 to O_2, the resistance drops down by a few orders of magnitude, and this change is temperature-sensitive. The resistance under O_2 or H_2 is much higher at low temperatures compared to high temperatures. The reduction under H_2 occurs in one step at high temperatures, however, at temperatures below ~400 °C it occurs in two steps (*i.e.*, a very sharp increase followed by a gradual decrease).

The observed resistance of the LBCO films under the flow of the redox gases can be understood by considering the average Co oxidation state. The resistance should be low when the average Co oxidation state is fractional (*e.g.*, +3.5 and +2.5) because it signals the presence of mixed valence cobalt ions (*e.g.*, Co^{3+}/Co^{4+} and Co^{2+}/Co^{3+}, respectively) and hence the occurrence of either hopping with low activation energy or

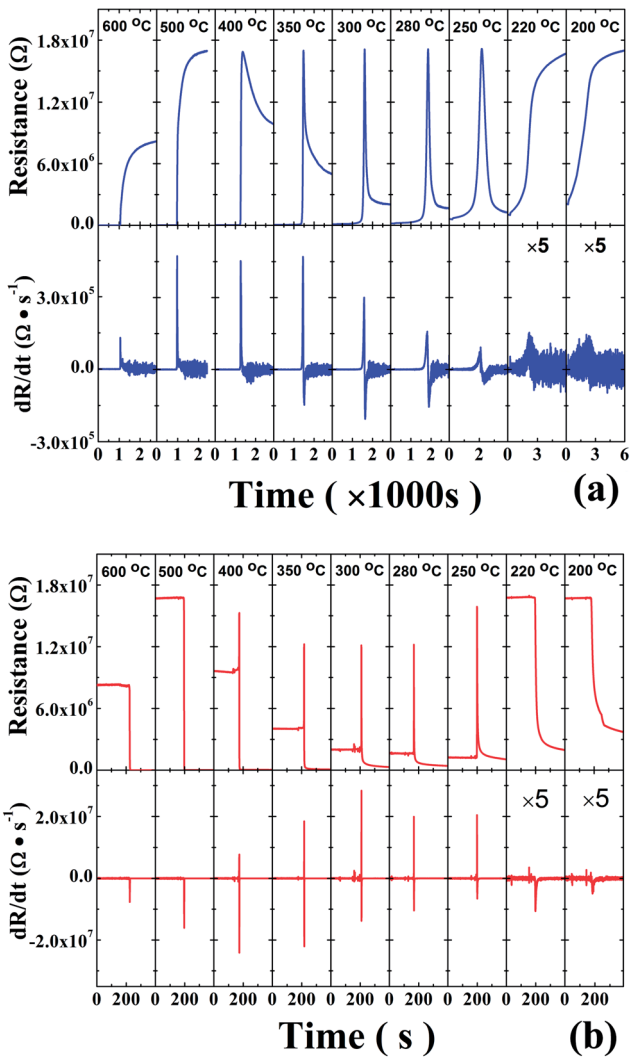

Fig. 3 Resistance changes *vs.* the gas flow time, *R vs. t*, of an epitaxial LBCO thin film: (a) during the reduction (under H_2) cycle at various temperatures and (b) during the oxidation (under O_2) cycle at various temperatures.

metallic conductivity. In contrast, the resistance of the LBCO films should be high when the average Co oxidation state is an integer (*e.g.*, +3 and +2) because electron-hopping is difficult in the case of single valence. The average Co oxidation state is +3.5 for $LaBaCo_2O_6$, +3 for $LaBaCo_2O_{5.5}$, and +2.5 for $LaBaCo_2O_5$. Our first principles density functional theory calculations for $LaBaCo_2O_6$ and various probable structures of $LaBaCo_2O_{5.5}$ and $LaBaCo_2O_5(OH)$, show that hydrogen atoms are present in LBCO as bound to oxygen forming O–H bonds. The average Co oxidation state is then +3 for $LaBaCo_2O_5(OH)$, and +2.5 for $LaBaCo_2O_{4.5}(OH)$, and +2 for $LaBaCo_2O_{3.5}(OH)_2$.

3.3. Redox equations

In general, any state transition of the LBCO thin films should arise from the chemical reactions. The reduction reaction of the LBCO thin films corresponding to their conducting-to-insulating transition can be expressed as

$$H_2 + O_O'' + 2Co^{4+} \rightarrow H_2O + 2Co^{3+} + V_O^{\cdot\cdot} + 2e^- \quad (1)$$

While the oxidation reaction corresponding to the insulating-to-conducting transition can be expressed as

$$O_2 + 2V_O^{\cdot\cdot} + 4Co^{3+} + 4e^- \rightarrow 2O_O'' + 4Co^{4+} \quad (2)$$

The LBCO thin films are stabilized at the insulating state with Co^{3+} ions under H_2 at medium temperatures, probably because the oxygen potential (*i.e.*, the Gibbs energy of formation ΔG)[34] of H_2O is lower than that of the LBCO films with Co^{4+} ions but higher than that of LBCO films with Co^{3+} ions. However, the oxygen potentials are temperature-dependent, so it is possible that the oxygen potential of H_2O might become lower than that of the LBCO films with Co^{3+} ions. In fact, a further reduction reaction of the LBCO thin films following the reaction (1) does continue according to the sudden change in the resistance at low temperatures. The further reduction reaction can be expressed as

$$H_2 + O_O'' + 2Co^{3+} \rightarrow H_2O + 2Co^{2+} + V_O^{\cdot\cdot} + 2e^- \quad (3)$$

where O_O'' is a lattice oxygen while $V_O^{\cdot\cdot}$ is an oxygen ion vacancy.

As a result of the reaction (3), the LBCO thin films are converted from an insulating to a conducting state, in which new small polarons might play the role of new carriers, as depicted in Fig 2(c). The oxidation reaction corresponding to the semiconducting-to-insulating transition can be expressed as

$$O_2 + 2V_O^{\cdot\cdot} + 4Co^{2+} + 4e^- \rightarrow 2O_O'' + 4Co^{3+} \quad (4)$$

3.4. Analysis of the cycling stability

Usually, changes in the oxygen vacancy concentration of the LBCO thin films are expected to bring about expansion, contraction or even destruction of their structures. Nevertheless, as shown in Fig. 2(a) and Fig. 4(a), the transitions among the different states have good reproducibility during five to seven reduction/oxidation cycles at low temperatures. The repeatable *R vs. t* curves in these cycles reflect a repeatable change in the oxygen vacancy concentration and the variation of the Co oxidation states. They also reveal the good stability of the chemical properties of the LBCO thin films under reducing/oxidizing environments. The latter may benefit from the stable frame structure of the epitaxial thin films. According to the neutron diffraction studies of Seddon *et al.*,[19] $LaBaCo_2O_{4.25}$ prepared by a low-temperature reduction of $LaBaCo_2O_5$, using NaH, contains cobalt in three distinct coordination

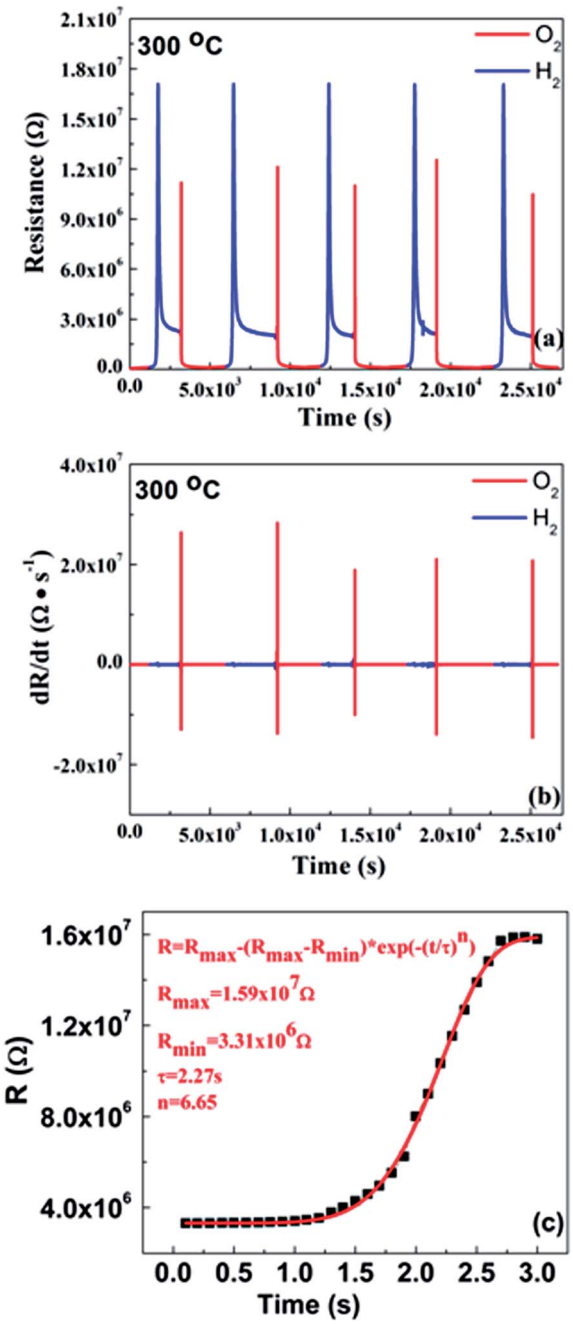

Fig. 4 Redox reactions of the LBCO thin films under the switching flow of a reducing/oxidizing gas flow at 300 °C: (a) *R vs. t* and (b) d*R*/d*t vs. t* curves. (c) Avrami analysis of the oxidation reactions associated with the oxidation state change from Co^{2+} to Co^{3+}.

environments, namely, CoO_4 tetrahedra (50%), CoO_5 square-pyramids (25%), and CoO_4 square-planes (25%). Owing to the weak reducing capacity of the H_2 environment, the oxygen vacancy concentration of the LBCO thin film under H_2 is much lower than that found for $LaBaCo_2O_{4.25}$. Thus, as shown in Fig. 5, it is probable that, in the LBCO thin films under H_2, CoO_4 tetrahedra or square planes are not present, but CoO_5 square pyramids are. Obviously, the expansion and contraction of the LBCO thin films would be much less for the change between the CoO_5 square pyramids and the CoO_6 octahedra than between the CoO_4 tetrahedra/square-planes and the CoO_6 octahedra.

3.5. Chemical dynamics analysis

From the perspective of the dR/dt *vs.* t curves, the LBCO thin films possess ultrafast chemical dynamics during the oxidation cycle, with the largest change above $10^7\ \Omega\ s^{-1}$ even at 300 °C, as shown in Fig. 4(b). In particular, the oxidation reaction (4) at 300 °C has a very short reaction time and a greater change in dR/dt than oxidation reaction (2) does at either 300 °C or 500 °C. The ultrafast oxidation from Co^{2+} to Co^{3+} can be understood as arising from the higher oxygen vacancy concentration and higher reducibility of the LBCO thin films with Co^{2+}.

To further understand the dynamic nature of the ultrafast oxidation from Co^{2+} to Co^{3+}, we analyzed our data by employing the Avrami equation.[35] For a solid-state phase transformation, the degree of its completion is defined as the volume fraction $f(t)$ of a new phase in the solid phase. A solid–gas reaction consists of several steps such as the adsorption of gaseous molecules on the surface of the solid, the dissociation of the molecules, and the atomic diffusion and nucleation. The rate of the reaction is determined by the slowest step. The volume fraction $f(t)$ as a function of the reaction time can be expressed as

$$f(t) = 1 - \exp[-(t/\tau)^n] \quad (5)$$

where $f(t)$ is the volume fraction, n the nucleation factor representing the nucleation type, and τ is the time for which $f(t) = 0$. Normally, $n = 4$ when nucleation occurs at a constant nucleation rate, $n = 3$ if the transformation is only the three-dimensional growth of the nuclei after the preformation of the nuclei, $n = 3$–4 if the nucleation rate decreases with time, and $n > 4$ if the nucleation rate increases with time. For the solid reaction dynamics, it is common to use the resistance change to calculate the volume fraction $f(t)$ as

$$f(t) = \frac{R_t - R_0}{R_1 - R_0} \quad (6)$$

where R_t, R_0, and R_1 indicate the resistance of the solid at time t, at the start ($t = 0$) and at the end of the reaction, respectively. For the oxidation reaction from Co^{2+} to Co^{3+}, the resistance increases from R_{min} to R_{max}. Thus, by using eqn (5) and (6), the resistance at time t can be expressed as

$$R = R_{max} - (R_{max} - R_{min}) \exp[-(t/\tau)^n] \quad (7)$$

The analysis of our data using eqn (7) indicates that the oxidation reaction at 300 °C is controlled by the nucleation rate, and the whole reaction can be completed in 3 seconds, as shown in Fig. 4(c).

The phase transition involving the change from the oxidation state $Co^{2+}$to Co^{3+} is highly dependent upon the oxidation temperature. The time constants and the nucleation factors obtained by fitting the resistance curves with eqn (7) are plotted in Fig. 6. The reaction rate for the transition from Co^{2+} to Co^{3+} increases with increasing temperature (from 260 to 350 °C). From the curve of n we can find that the nucleation type also varies entirely with temperature. The extraordinary values of $n \gg 4$ signify that a large number of oxygen vacancy sites, which act as potential oxidation nucleation centers, are generated during the reduction process above 300 °C. At 280 °C, nucleation only occurs at the start of the transformation. At 260 °C, the oxidation process from Co^{2+} to Co^{3+} is reduced in reaction rate and is not nucleation-controlled any longer.

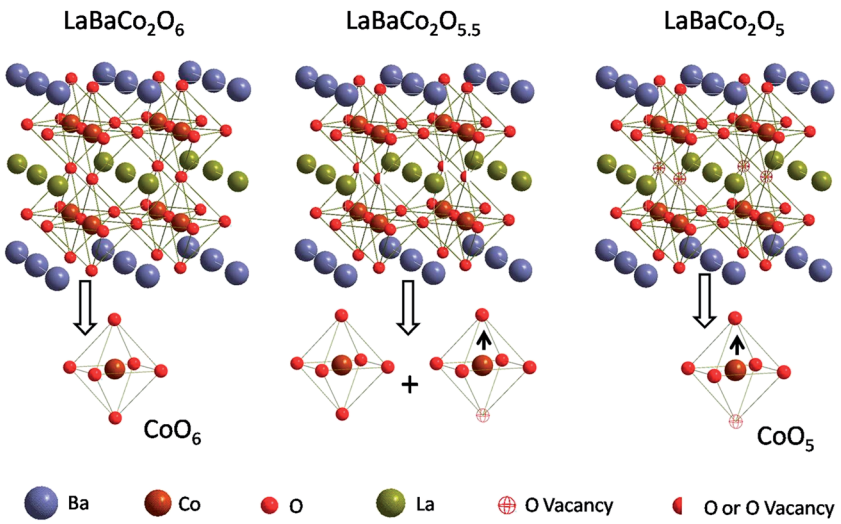

Fig. 5 Polyhedral representations of the crystal structures of $LaBaCo_2O_6$, $LaBaCo_2O_{5.5}$ and $LaBaCo_2O_5$.

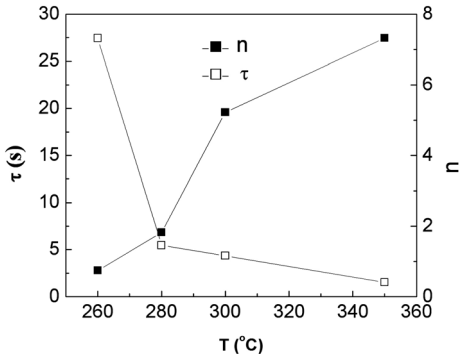

Fig. 6 The n and τ values obtained from the Avrami analysis for the oxidation reactions associated with the change in the Co oxidation state, $Co^{2+}$to Co^{3+}, at temperatures between 260 and 350 °C.

4. Conclusions

The redox dynamics of the epitaxial LBCO thin films exposed to the switching flow of H_2 and O_2 gases at 260–700 °C were systematically studied by ac resistance measurements. At medium temperatures (400–700 °C), LBCO thin films are sensitive to the reducing/oxidizing environments, exhibiting a conducting-to-insulating transition in each oxidation/redox cycle. At low temperatures (260–350 °C) under a H_2 environment, the LBCO thin films undergo a conducting-to-insulating-to-conducting transition, which corresponds to the variation of the oxidation states, Co^{4+}/Co^{3+} to Co^{3+} to Co^{3+}/Co^{2+}. The oxidation reaction from Co^{2+} to Co^{3+} at low temperatures is faster than that from Co^{3+} to Co^{4+}. The time required to change from the Co^{2+} to Co^{3+} state decreases from 30 to 3 s when the temperature is increased from 260 to 350 °C. The nucleation rate of the reaction at 300 and 350 °C increases with time during their very short reaction process. The ultrafast redox reactions at 300–700 °C indicate that the epitaxial LBCO thin films are promising candidates for low-temperature SOFC cathodes, chemical gas sensors, effective deoxidizers, and vehicle exhaust catalysts.

Acknowledgements

This research was partially supported by the Department of Energy under DE-FE0003780 and the National Science Foundation under NSF-NIRT-0709293 and NSF-PREM DMR-0934218. Also, HBW, SYB, CRM and ML would like to acknowledge the support from the "China Scholarship Council" for the program of national study-abroad project for the postgraduates of high level universities at UTSA.

References

1 S. Roy, I. S. Dubenko, M. Khan, E. M. Condon, J. Craig, N. Ali, W. Liu and B. S. Mitchell, *Phys. Rev. B: Condens. Matter Mater. Phys.*, 2005, **71**, 024419.
2 A. Maignan, V. Caignaert, B. Raveau, D. Khomskii and G. Sawatzky, *Phys. Rev. Lett.*, 2004, **93**, 026401.
3 T. Hibino, A. Hashimoto, T. Inoue, J.-i. Tokuno, S.-i. Yoshida and M. Sano, *Science*, 2000, **288**, 2031.
4 V. V. Kharton, S. B. Li, A. V. Kovalevsky, A. P. Viskup, E. N. Naumovich and A. A. Tonoyan, *Mater. Chem. Phys.*, 1998, **53**, 6.
5 N. P. Brandon, S. Skinner and B. C. H. Steele, *Annu. Rev. Mater. Res.*, 2003, **33**, 183.
6 A. Tarancón, A. Morata, G. Dezanneau, S. J. Skinner, J. A. Kilner, S. Estradé, F. Hernández-Ramírez, F. Peiró and J. R. Morante, *J. Power Sources*, 2007, **174**, 255.
7 A. Tarancon, S. J. Skinner, R. J. Chater, F. Hernandez-Ramirez and J. A. Kilner, *J. Mater. Chem.*, 2007, **17**, 3175.
8 A. Chang, S. J. Skinner and J. A. Kilner, *Solid State Ionics*, 2006, **177**, 2009.
9 N. Li, Z. Lü, B. Wei, X. Huang, K. Chen, Y. Zhang and W. Su, *J. Alloys Compd.*, 2008, **454**, 274.
10 C. Frontera, A. Caneiro, A. E. Carrillo, J. Oró-Solé and J. L. García-Muñoz, *Chem. Mater.*, 2005, **17**, 5439.
11 A. A. Taskin, A. N. Lavrov and Y. Ando, *Appl. Phys. Lett.*, 2005, **86**, 091910.
12 G. Kim, S. Wang, A. J. Jacobson, L. Reimus, P. Brodersen and C. A. Mims, *J. Mater. Chem.*, 2007, **17**, 2500.
13 G. Kim, S. Wang, A. J. Jacobson, Z. Yuan, W. Donner, C. L. Chen, L. Reimus, P. Brodersen and C. A. Mims, *Appl. Phys. Lett.*, 2006, **88**, 024103.
14 J. Liu, G. Collins, M. Liu, C. L. Chen, J. He, J. C. Jiang and E. I. Meletis, *Appl. Phys. Lett.*, 2012, **100**, 193903.
15 E.-L. Rautama, P. Boullay, A. K. Kundu, V. Caignaert, V. Pralong, M. Karppinen and B. Raveau, *Chem. Mater.*, 2008, **20**, 2742.
16 E.-L. Rautama, V. Caignaert, P. Boullay, A. K. Kundu, V. Pralong, M. Karppinen, C. Ritter and B. Raveau, *Chem. Mater.*, 2008, **21**, 102.
17 I. O. Troyanchuk, D. V. Karpinsky, M. V. Bushinsky, V. Sikolenko, V. Efimov and A. Cervellino, *JETP Lett.*, 2011, **93**, 139.
18 A. Maignan, C. Martin, D. Pelloquin, N. Nguyen and B. Raveau, *J. Solid State Chem.*, 1999, **142**, 247.
19 J. Seddon, E. Suard and M. A. Hayward, *J.Am. Chem. Soc.*, 2010, **132**, 2802.
20 J. Liu, M. Liu, G. Collins, C. L. Chen, X. N. Jiang, W. Gong, A. J. Jacobson, J. He, J. C. Jiang and E. I. Meletis, *Chem. Mater.*, 2010, **22**, 799.
21 J. Liu, G. Collins, M. Liu, C. L. Chen, J. Jiang, E. I. Meletis, Q. Zhang and C. Dong, *Appl. Phys. Lett.*, 2010, **97**, 094101.
22 M. Liu, J. Liu, G. Collins, C. R. Ma, C. L. Chen, J. He, J. C. Jiang, E. I. Meletis, A. J. Jacobson and Q. Y. Zhang, *Appl. Phys. Lett.*, 2010, **96**, 132106.
23 M. Liu, C. R. Ma, J. Liu, G. Collins, C. L. Chen, J. He, J. C. Jiang, E. I. Meletis, L. Sun, A. J. Jacobson and M.-H. Whangbo, *ACS Appl. Mater. Interfaces*, 2012, **4**, 5524.
24 J. He, J. C. Jiang, J. Liu, M. Liu, G. Collins, C. R. Ma, C. L. Chen and E. I. Meletis, *Thin Solid Films*, 2011, **519**, 4371.
25 C. R. Ma, M. Liu, G. Collins, J. Liu, Y. M Zhang, C. L. Chen, J. He, J. C. Jiang and E. I. Meletis, *Appl. Phys. Lett.*, 2012, **101**, 021602.

26 C. R. Ma, M. Liu, G. Collins, H. B. Wang, S. Y. Bao, X. Xu, E. Enriquez, C. L. Chen, Y. Lin and M.-H. Whangbo, *ACS Appl. Mater. Interfaces*, 2012, **5**, 451.
27 Z. Yuan, J. Liu, C. L. Chen, C. H. Wang, X. G. Luo, X. H. Chen, G. T. Kim, D. X. Huang, S. S. Wang, A. J. Jacobson and W. Donner, *Appl. Phys. Lett.*, 2007, **90**, 212111.
28 J. Liu, G. Collins, M. Liu and C. L. Chen, *APL Mater.*, 2013, **1**, 031101.
29 S. Y. Bao, C. R. Ma, G. Chen, X. Xu, E. Enriquez, C. L. Chen, Y. M. Zhang, J. L. Bettis, M.-H. Whangbo, C. Dong and Q. Y. Zhang, *Sci. Rep.*, 2014, **4**, 4726.
30 D. Emin and T. Holstein, *Ann. Phys.*, 1969, **53**, 439.
31 S. Mollah, H. L. Huang, H. D. Yang, S. Pal, S. Taran and B. K. Chaudhuri, *J. Magn. Magn. Mater.*, 2004, **284**, 383.
32 X. J. Chen, C. L. Zhang, C. C. Almasan, J. S. Gardner and J. L. Sarrao, *Phys. Rev. B: Condens. Matter Mater. Phys.*, 2003, **67**, 094426.
33 T. Koslowski, *Phys. Chem. Chem. Phys.*, 1999, **1**, 3017.
34 M. Olette and M. F. Ancey-Moret, *Rev. Mét.*, 1963, **60**, 569.
35 M. Avrami, *J. Chem. Phys.*, 1939, **7**, 1103.